Solidification Sequence and Evolution of Microstructure During Rheocasting of Four Al-Si-Mg-Fe Alloys with Low Si Content

MOSTAFA PAYANDEH, ANDERS E.W. JARFORS, and MAGNUS WESSÉN

Four Al-Si-Mg-Fe alloys with Si contents varying from 1.6 to 4.5 wt pct were rheocast, using the RheoMetal™ process to prepare slurry and cast in a vertical high-pressure die casting machine. Particle size and Si concentration in the α-Al particles in the slurry and in the as-rheocast component were investigated. A uniform distribution of Si in the globular α_1-Al particles was achieved in the slurry. In the rheocast samples, measurement of the α_1-Al particles showed that these particles did not increase significantly in size during pouring and secondary solidification. The two additional α-Al particles types, α_2-Al particles and α_3-Al particles, were identified as being a result of two discrete nucleation events taking place after slurry production. The Si concentration in the α_2-Al and α_3-Al particles indicated that the larger α_2-Al particles precipitated before the α_3-Al particles. In addition, in the as-rheocast condition, the Si distribution inside the α_1-Al particles showed three distinct zones; an unaffected zone, a transition zone, and in some cases the start of a dendritic/cellular zone. The phenomenon of dendritic growth of globular α_1-Al particles during secondary solidification occurred concomitantly with the final eutectic reaction and increased with increasing amount of the Al-Si eutectic phase.

I. INTRODUCTION

MICROSTRUCTURAL characteristics such as segregation patterns and porosity in a cast material have a significant influence on both material properties and post solidification processing, for instance heat treatment. In cast materials, the microstructure is also strongly influenced by the mold filling process, and solidification of metals as a sequence of nucleation and subsequent growth of solids.[1] For high-pressure die casting (HPDC) processes, solidification of the melt starts as the liquid is poured into a cold shot chamber followed by injection into the die cavity. Formation of a new solid particles in the shot chamber has been observed by Laukli[2] and related to the level of undercooling based on the superheat of the melt and temperature of the shot chamber. The filling time in the HPDC process is typically in the order of tens of milliseconds and flow is turbulent, resulting in air entrapment and porosity.[3]

Semi-Solid Metal (SSM) processing integrated with HPDC is a new casting method that has established itself as a promising technology to produce high-quality components with sound microstructure.[4] In rheocasting, a variant of SSM casting,[5] solidification starts by decreasing the melt temperature below the liquidus under intensive shearing, thereby forming a slurry typically with a non-dendritic primary phase.[6] The preformed slurry is stabilized at a fixed temperature (slurry temperature) before the die filling process. Recent investigations of the microstructure in an SSM cast component revealed that different sizes of α-aluminum particles formed during casting, which indicates a multistage solidification process.[7] Partial solidification of the melt during cooling under intense shearing results in the formation of globular particles in a slurry with a uniform temperature and species, for instance Si, distribution throughout the remaining liquid phase.

The preformed solid particles in the slurry increase the viscosity and cause a thixotropic flow during filling,[8] which reduces the total amount of defect formed by reducing air entrapment in the cast material. The rheological properties of the slurry reduce turbulent flow during die cavity filling as compared to traditional liquid casting, thereby decreasing the porosity formation that originates from entrained air. Furthermore, the spherical morphology of the solid particles increases the critical solid fraction at which the slurry turns coherent compared to liquid casting, and the melt in the interdendritic region is reduced compared to what it would be possible to cast following the standard HPDC process.[9] The different filling and solidification process in rheocasting will result in a different microstructure as compared to the traditional HPDC process.

The morphological evolution during SSM casting has been studied in different SSM casting processes. In the

MOSTAFA PAYANDEH, Ph.D. Student, ANDERS E.W. JARFORS, Professor, and MAGNUS WESSÉN, Associate Professor, are with the Department of Materials and Manufacturing, School of Engineering, Jönköping University, Box 1026, 551 11, Jönköping, Sweden. Contact e-mail: mostafa.payandeh@ju.se

most of these studies, the effect of forced convection has been considered on transition of morphology of primary phase from dendritic to globular *via* rosette shape.[10–13] On the other hand, despite of these studies, there is still lack of information to understanding, the effect of slurry preparation stage on solidification process and solute distribution in final rheocast components. This lack of information is partially related to the different heat extraction methods used for slurry preparation.[14–16] For instance, in some rheocasting processes, an internal cooling agent is used.[17] RheoMetal™ is such a process, where internal cooling is achieved by a melting metal body, often denominated as an enthalpy exchange material (EEM), which is attached to a stirrer.[18] The fact that the EEM is used makes the RheoMetal™ process a hybrid SSM process. The slurry is partly formed by rheo-processing from the solidification of the melt and partly by thixo-processing as the EEM is melting.[19] This makes the RheoMetal™ different from other rheocasting processes.

The formation of slurry includes a melting process as well as a spheroidisation process, which has been reported earlier.[20] The study on melting of EEM showed that the solid particles in slurry could come from EEM or solid phase formed during stirring of EEM.[19] Because of this, the primary fraction formed is far from equilibrium and this offers a new opportunity to a create slurry from aluminum alloys with short freezing ranges. In RheoMetal™ processing, the solid fraction can be up to ten times larger than that predicted from the alloy composition and final slurry temperature assuming Scheil segregation.[21]

In the present study, the solidification sequence and microsegregation patterns in quenched slurry as well as rheocast components produced using the RheoMetal™ process were investigated to better understand the nature of this deviation from equilibrium. The influence of the solidification sequence on microstructural characterisics and microsegregation patterns of four different Al-Si-Mg-Fe alloys with Si contents from 1.6 to 4.5 wt pct were investigated.

II. EXPERIMENTAL

A. RheoCasting

Experiments were made using a manual RheoMetal™ set-up[18] to prepare the slurry from four different low Si-containing aluminum alloys. The compositions of the alloys are detailed in Table I. The alloys were produced in batches of 50 kg using a resistance furnace. The process started with ladling 3 kg of melt, of which a small portion was cast into a simple cylindrical mold to create the EEM as shown in Figure 1. Based on the pre-experiment results on the effect of EEM amount and superheat on solid fraction of slurry, the EEM amount and superheat were set at 6 pct of the shot weight and 20 K to 25 K, respectively, to obtain 50 pct solid fraction. The remaining melt in the ladle was then used to prepare a slurry. A previously manufactured EEM, attached to a steel rod, was then inserted under stirring into the melt. The stirring continued for 15 to 20 seconds at 900 rpm to ensure that the EEM had melted completely and produced a slurry. The temperature of the melt was measured using a K-type thermocouple during slurry preparation. After preparation of the slurry, a small sample to study the microstructure prior to rheocasting was prepared by rapid quenching.

The slurry was subsequently cast using a 50-ton cold chamber Vertical Pressure Die Casting (VPDC) machine with a vertically clamped tool. The die temperature was controlled using a PolyTemp™ oil heater. The die surface temperature was measured as 473 K to 493 K (200 °C to 220°C) using IR thermometer and maintained in this interval throughout the experiments. Figure 2 schematically illustrates the sequence of four steps in the VPDC machine as well as ejection of the final component. As the shot sleeve docks with the fixed mold half by means of rotation and upward motion, the slurry was injected into the die cavity. To minimize turbulence in the injection step, the plunger speed was set to 0.1 m/second, which resulted in a gate speed of 1 m/second and a fill time of approximately 1 s. The ejector pins in the moving half of the mold ejected the part. A schematic illustration of the final rheocast component is shown in Figure 3.

B. Sampling and Measurements

Samples for microstructural evaluation from all castings were taken from the same position in the center of the components and cut parallel to the filling direction to ensure repeatable and comparable conditions, as shown schematically in Figure 3. The samples were prepared using standard metallographic techniques and etched using a 10 pct NaOH solution and Struers™ OP-S suspension for 5 minutes to maximize contrast between the different phases under optical microscope observation.[22] Microstructural characterization was performed using an Olympus™ optical microscope and the Olympus Stream™ image analysis system. Particles size measurements based on image contrast were made on at least 5 representative images and 100 α-Al particles in total from each sample. To

Table I. Chemical Compositions of the Four Alloys Investigated (Mass Percentage)

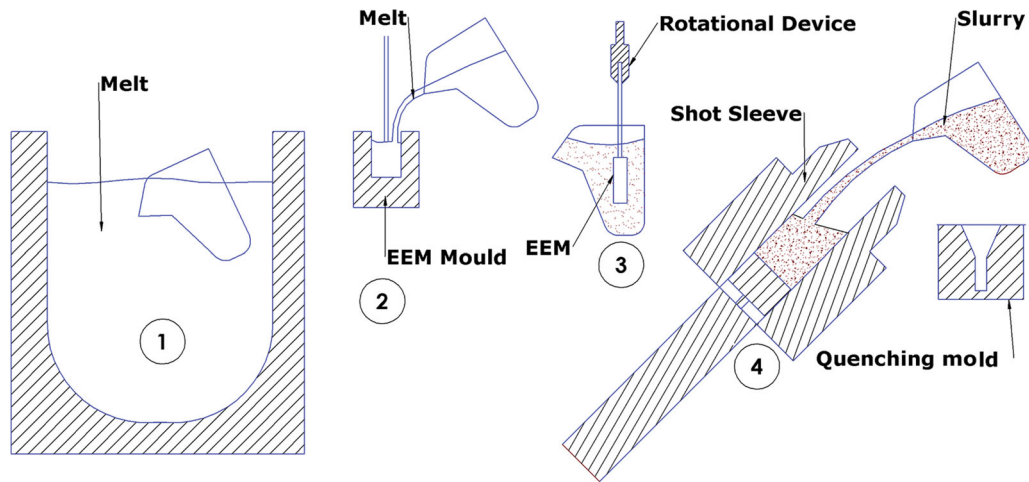| Alloy	Si	Fe	Cu	Mn	Mg	Zn	T_L [K (°C)]
1	1.69	0.80	<0.01	<0.01	0.39	<0.01	919 (646)
2	2.49	0.80	<0.01	<0.01	0.40	<0.01	911 (638)
3	3.67	0.75	<0.01	<0.01	0.41	<0.01	907 (634)
4	4.56	0.75	<0.01	<0.01	0.40	<0.01	899 (626)

Fig. 1—Manual RheoMetal™ process; (1) extract the melt, (2) pour into a mold to make EEM, (3) prepare a slurry by means of stirring and EEM melting (4) pour the slurry into the shot chamber.
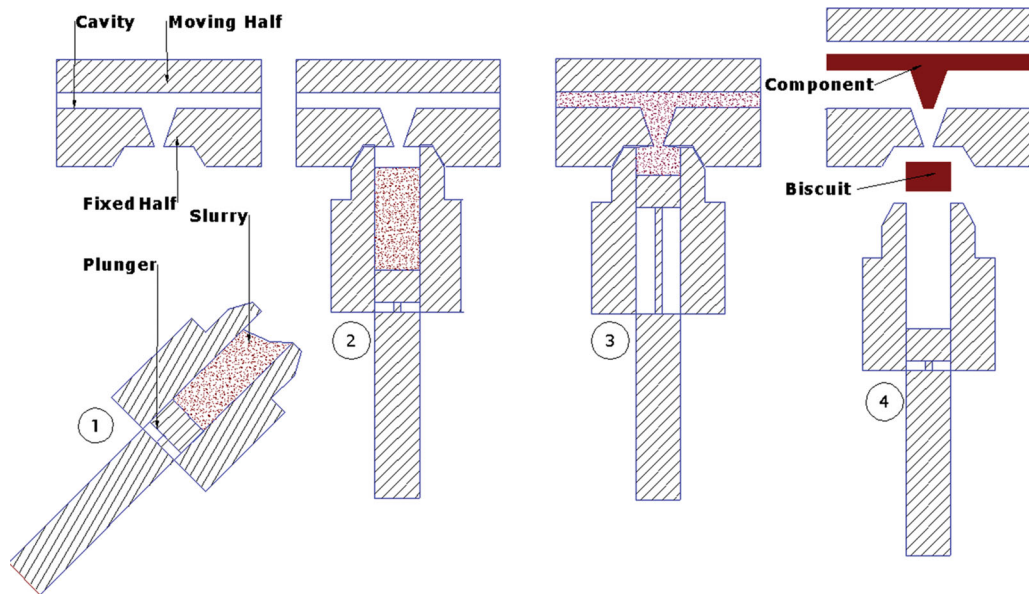

Fig. 2—Four steps of VPDC casting; (1) charge the chamber (2) docking (3) injection (4) punching biscuit and part ejection.

distinguish between slurry particles and other secondary microstructural features, a particle size discrimination technique was used.

The Si concentration in the aluminum phase was measured using a scanning electron microscope (SEM) equipped with an EDAX Apollo™ wavelength dispersive spectrometer (WDS). Pure elements were used as standards, and the acceleration voltage was set to 10 kV for the measurement of both Al- and Si-concentration. The compositions of the remaining melt after the slurry preparation stage in the quenched samples of the slurry and also of the precipitated phases in the cast component were defined by using five independent energy-dispersive X-ray spectroscopy (EDS) measurements in the SEM machine using a fixed accelerating voltage of 15 kV. The solubility limit of Si in aluminum for different conditions was calculated by ThermoCalc™[23] software, using the TCAL database.[24]

In order to use a consistent nomenclature, the globular primary α-Al particles formed during slurry preparation will be referred to as α_1-Al particles, while secondary and ternary particles formed during subsequent solidification during filling and cooling in the mold cavity will be referred to as α_2-Al and α_3-Al particles, respectively. The Si concentration in the α-Al phase will be given as C_{Si}^A, where A is the position related to the measured point in the α-Al phase particle, thereafter succeeded by the type of particle.

III. RESULTS

A. Microstructural Characteristics

The quenched slurry samples were taken at temperatures of 914 K, 905 K, 898 K, 892 K (641 ± 1 °C, 632 ± 1 °C, 625 ± 1 °C and 619 ± 2 °C) for alloys 1 through 4, respectively. Metallographic analysis of the quenched slurry samples was carried out on the middle section of the samples. The microstructure of quenched slurry sample for alloy 1 is shown in Figure 4(a). The results from microscopic investigation revealed that the globular α_1-Al particles clearly visible in a quenched liquid matrix (here present in the form of a fine dendritic morphology) for all alloys. After injection of the slurry into the cavity, the remaining melt solidified in a secondary solidification process, which occurred both during pouring into the cold chamber and inside the die cavity. In contrast to the primary solidification of α_1-Al particles (which occurs during slurry preparation), secondary solidification of the remaining melt takes place at higher cooling rates and under low or no shear forces. The microstructural features of the samples in the center region of the as-cast component made in alloy 4 are illustrated in Figure 4(b). In the rheocast samples, α_1-Al particles concentrate to the core region of component in agreement with previous findings by Laukli et al.[25]

The average diameter of the α_1-Al particles is collated in Table II. Quantitative metallography revealed that the formation and size of the primary α_1-Al depend on concentration of alloying elements in the slurry. The results from the metallographic examination also made it clear that there is no significant difference in size of α_1-Al particles, when comparing the microstructure in the as-rheocast component with that in the quenched slurry. Therefore, this confirms that almost no significant growth of α_1-Al particles takes place during secondary solidification.

At the high cooling rate provided by the die, nucleation inside the die cavity is expected to take place throughout the entire volume of the remaining liquid, resulting in smaller α-Al particles throughout the microstructure, as shown in Figure 5(a). These particles can be categorized according to their size into two main groups. The particles identified as α_2-Al particles, with a rosette shape, had sizes of the order of 25 μm, while the α_3-Al particles, which are rounded, were of the order of 10 μm. In the final stage of solidification, the remaining melt solidifies in a eutectic reaction. Figure 5(b) shows a typical microstructure of the eutectic phase in the alloy 4. The amount of eutectic appears to increase with increased alloy content. The EDS analysis results together with the morphology of the iron-rich confirms that β(AlFeSi) particles were formed. Additionally, the Al–Si eutectic in all four alloys was a fine-scaled eutectic with larger β(AlFeSi) particles present.

B. Element Concentration in the Precipitated Particles

1. α_1-Al particles in the quenched slurry

The concentration and distribution of Si in the α_1-Al particles in the quenched slurry were measured using WDS. Figure 6(a) illustrates the mapping line where Si
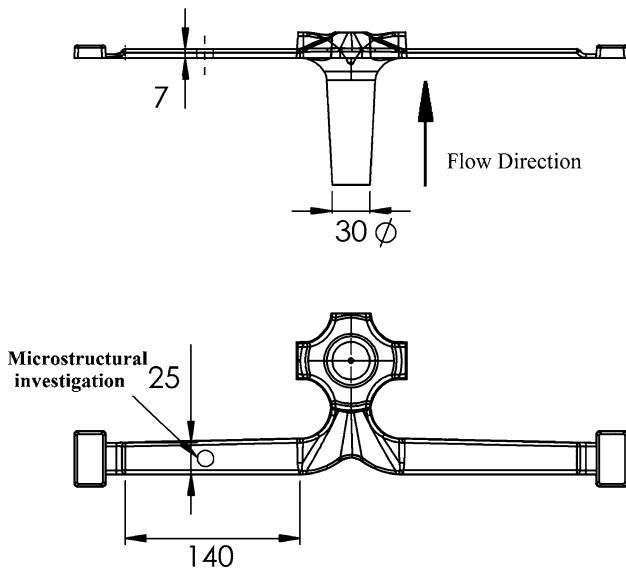

Fig. 3—Schematic diagram of half of the final rheocast component (all dimensions in mm).
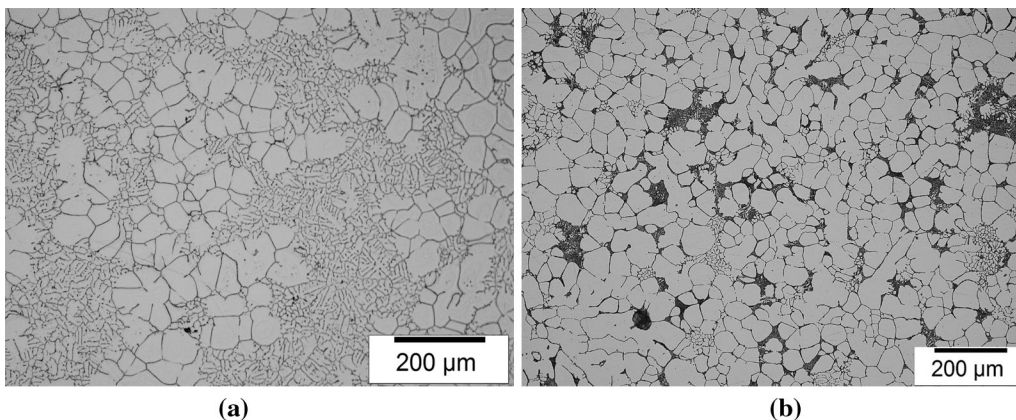

(a)

(b)

Fig. 4—Optical photomicrograph showing the typical microstructure for (a) a quenched slurry sample, alloy 4 and (b) a rheocast component in the core region, alloy 4.

Table II. Average Diameter of the -Al Particles (μm) in the Quenched Slurry and the Rheocast Samples

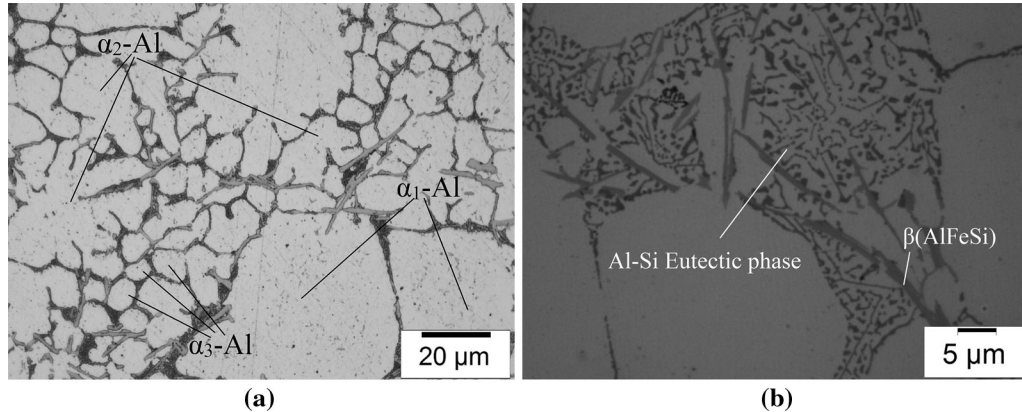| Alloy	α_1-Al in quenched samples (μm)	α_1-Al in as-cast component (μm)	α_2-Al in as-cast component (μm)	α_3-Al in as-cast component (μm)
1	74 ± 6	75 ± 8	28 ± 4	14 ± 3
2	68 ± 7	72 ± 8	26 ± 2	12 ± 2
3	64 ± 6	66 ± 8	25 ± 5	12 ± 4
4	60 ± 4	64 ± 9	27 ± 3	11 ± 6

Fig. 5—Optical micrographs showing (*a*) the typical microstructure of a rheocast component in the core region and formation of additional α_2-Al and α_3-Al particles (*b*) optical microscopy showing the typical eutectic region in the alloy 4.

concentration was measured in a α_1-Al particle. Five points on a straight line from the center to the surface were measured for each particle. The validity of the results was confirmed by measuring replicate points at different locations in the particle but at the same distance from the center. As shown in Figure 6(b), the Si concentration was nearly constant across the α_1-Al particles, this being a key observation. The Si concentration inside the α_1-Al particles increased as the Si content in the alloy was increased. Measurements on different areas of the α_1-Al particle in each alloy confirmed that the Si concentration was almost identical at identical distances from the particle central point.

Furthermore, the composition of the liquid portion of the slurry was measured using EDS. The results for Si, Mg, and Fe are collated in Table III. The measurement error was calculated based on multiple measurements in different areas. The small standard deviation indicates a uniform distribution of alloying elements. The measurement indicates higher concentration of main alloying elements in the liquid portion of the slurry.

2. α_1-Al particles in the as-rheocast condition

The distribution of Si in α_1-Al particles in the as-rheocast samples was measured using WDS. Two particles from alloys 1 and 4 are shown in Figure 7(a) and Figure 7(b), respectively. An important feature of the selected particles was that one side was separated from an adjacent α_1-Al particle by only a very thin layer of eutectic β(AlFeSi). This will be referred to as the "adjacent-to-globular side", and another side was close to the eutectic which will be referred to as the "adjacent-to-eutectic side". As Figure 7 illustrates, the concentration of Si was measured from the adjacent-

to-globular side of the α_1-Al particles to the adjacent-to-eutectic side. The additional points were measured in the boundary and the critical area by considering the distance from the surface of the particle. The error measurement shows that the maximum difference for points in the identical positions is around ±0.03 wt pct for all alloys.

Figures 8(a) through (d) shows the results from the WDS measurements as concentration profiles of Si in the α_1-Al particles in the as-rheocast condition. Based on these profiles, two different zones for alloy 1 and three different zones for alloys 2 to 4 were distinguishable. The central *unaffected zone* of the α_1-Al particles has a near constant concentration of Si, similar to that observed in the as-quenched condition in the slurry (Figure 6(b)), and the Si concentration increased in the region near to the surface of the α_1-Al particles, the so-called *transition zone*. The transition zones in different alloys were not identical and the width of the transition zone depended on alloy composition, increasing with increasing amounts of Si in the alloy. Furthermore, the width of the transition zone in adjacent-to-globular side and adjacent-to-eutectic side of the particles was different.

The most noticeable difference between the morphology of α_1-Al particles in the as-quenched condition, see Figure 6(a), and in the as-rheocast samples, see Figure 7, was the growth of a dendritic/cellular zone in the adjacent-to-eutectic side surface of α_1-Al particles. The Si concentration in this part of the α_1-Al particles, Figure 8, showed a further increase as compared to the transition zone. In the adjacent-to-globular side in which the eutectic phase has no chance to grow, the result shows no dendritic growth occurred and back
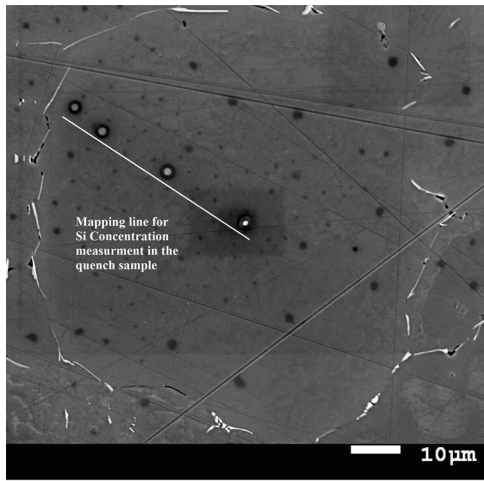
(a)
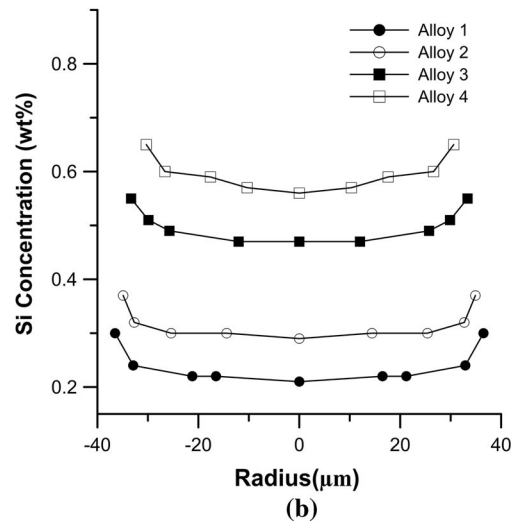
(b)

Fig. 6—(a) Mapping line where Si concentration was measured (b) the results of measurement show Si concentration through globular α_1-Al particles for quenched samples of each alloy.

Table III.   Chemical Compositions of Remaining Melt in the Quenched Sample (Weight Percent) Using EDS Measurement

Alloy	Si (Weight Percent)	Fe (Weight Percent)	Mg (Weight Percent)	T_M [K (°C)]
1	2.72 ± 0.42	1.45 ± 0.28	0.59 ± 0.04	910 (637)
2	4.13 ± 0.32	1.41 ± 0.19	0.57 ± 0.06	902 (629)
3	5.87 ± 0.28	1.32 ± 0.29	0.59 ± 0.02	892 (619)
4	8.56 ± 0.39	1.38 ± 0.33	0.61 ± 0.07	878 (605)
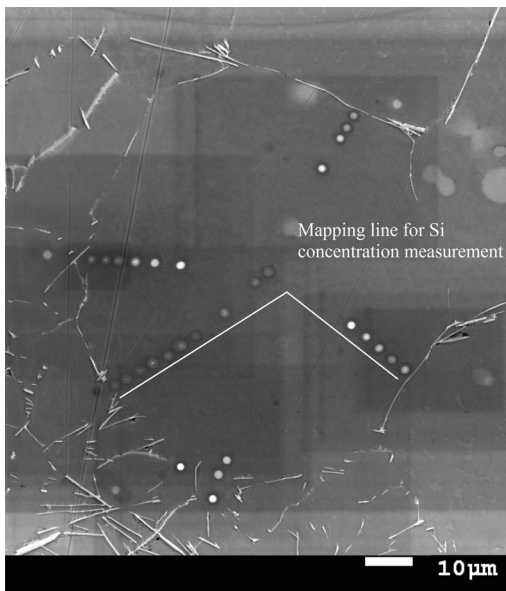
(a)
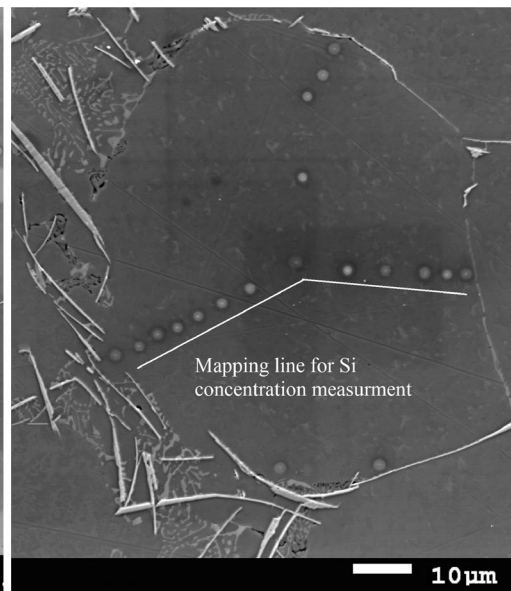
(b)

Fig. 7—Microstructure of a representative α_1-Al particle used in the measurement of the Si concentration profile in the as-rheocast state for (a) alloy 1 and (b) alloy 4 (lines are added as a guide to the eye).

diffusion of Si at high temperature can explain the transition zone. The shorter time available for Si diffusion resulted in a narrower transition zone compared to the transition zone formed on the adjacent-to-eutectic side. This scenario was observed in all four alloys.
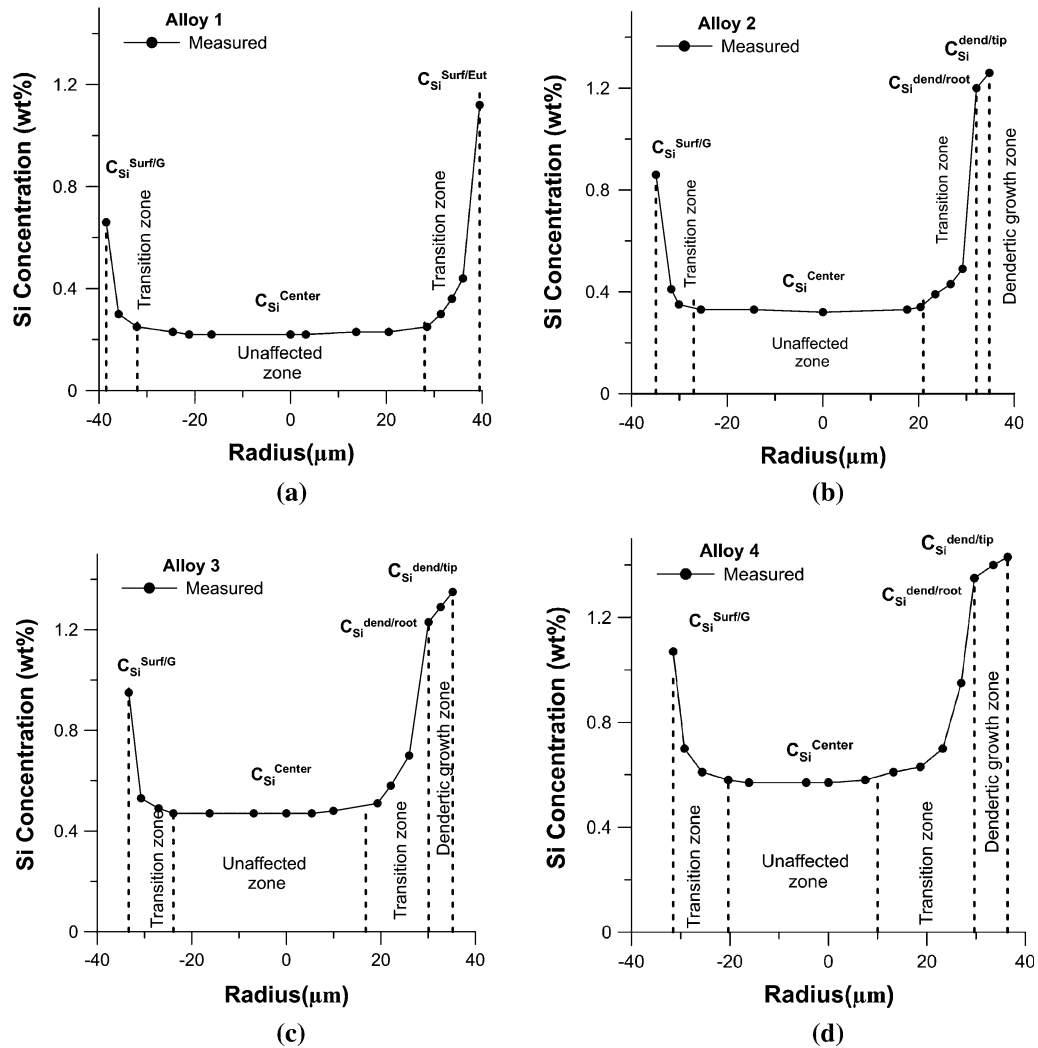
Fig. 8—The segregation profile of Si in of α_1-Al particles for (*a*) alloy 1 (*b*) alloy 2 (*c*) alloy 3 (*d*) alloy 4 in the rheocast samples.

3. α_2-Al and α_3-Al particles in the as-rheocast alloy

As the slurry enters the die cavity, the remaining melt starts to solidify. In the as-rheocast material, α_2-Al and α_3-Al particles were observed. These were not seen in the quenched slurry samples and must therefore have formed after the slurry was poured into the shot sleeve. Particles from α_2-Al and α_3-Al phases were selected in each sample. By means of WDS, the Si concentrations were measured at two positions—in the center and at the surface of α_2-Al particles, Figure 9 and at one position in the center of α_3-Al particles. The Si concentrations in α_2-Al and α_3-Al particles are shown in Figure 10. The average Si concentration in the center of α_2-Al particles, Figure 10(a), showed higher values than those found in the center of the α_1-Al particles but lower than those measured in the center of the α_3-Al particles. The Si concentration close to the edge of the α_2-Al particles was very close to the Si solubility at the eutectic point for alloys 3 and 4, Figure 11.
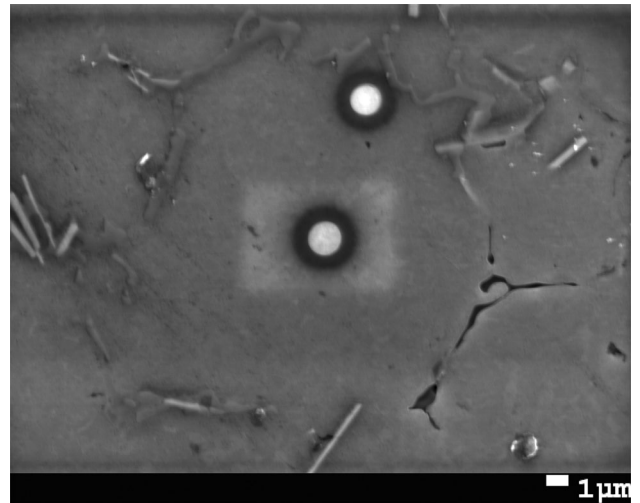

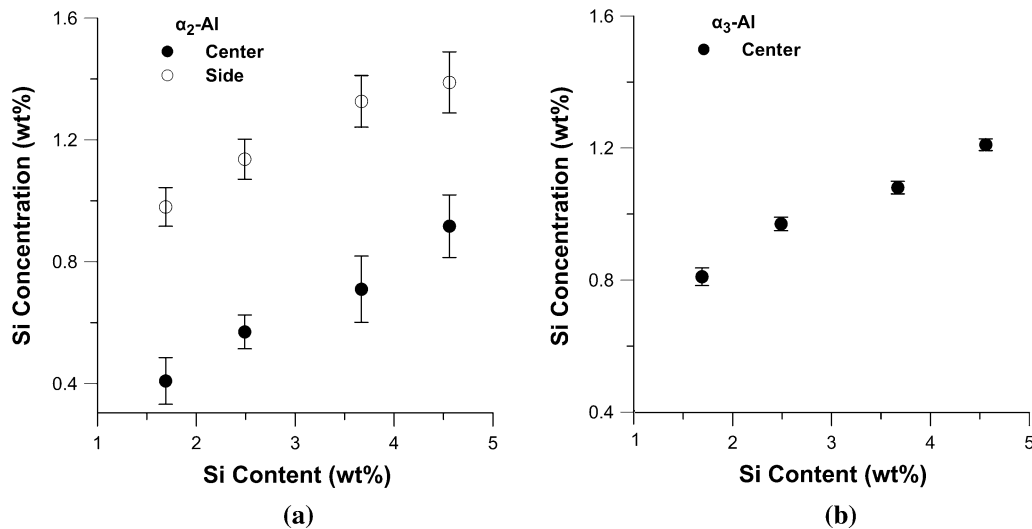Fig. 9—Si concentration measuring positions in α_2-Al particles.

Fig. 10—(a) The measured Si concentration in the center and at the side of α_2-Al particles in the range size of 20 to 30 μm and (b) at the center of α_3-Al particles in the range size of 5 to 10 μm.
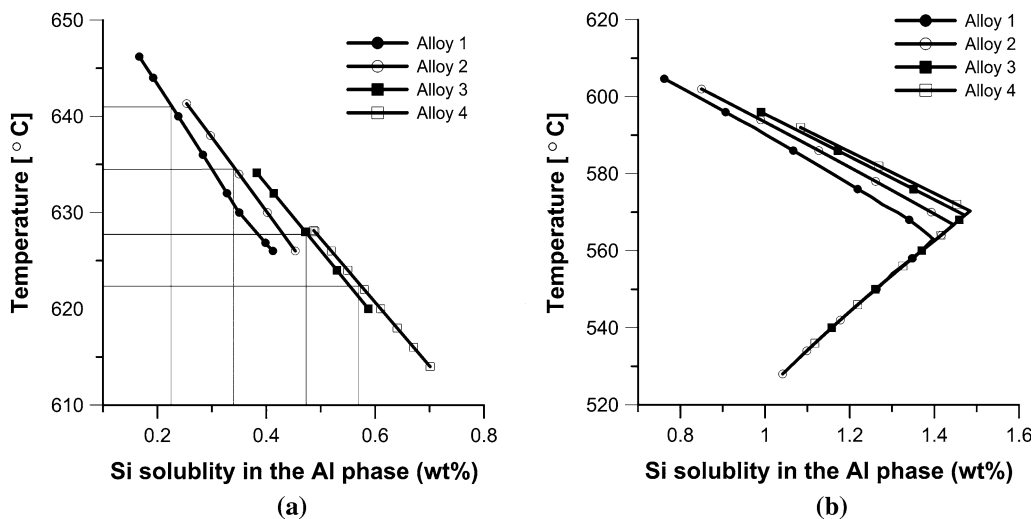

Fig. 11—The solubility of Si in the aluminum solid phase in the four alloys as a function of temperature, calculated using ThermoCalc™ (a) in the temperature range for the slurry preparation, (b) in the temperature range of formation the of α_2-Al and α_3-Al particles.

IV. DISCUSSION

A. The Sequence and Mechanism of Particle Formation

Assuming that larger particles require more time to grow, it could, as an initial suggestion be postulated that the formation sequence was α_1-Al, α_2-Al- and α_3-Al. The presence of the α_1-Al particles in the quenched slurry samples clearly indicates the formation of these particles in the slurry production process. The α_1-Al particles showed no statistically significant growth during the rheocasting process. It is however clear that Si diffusion took place, as indicated by the Si concentration profile from the quenched slurry to the as-rheocast material in the transition layer.

In order to establish the sequence of nucleation events, it is necessary to identify at which temperature the particles have formed, as the post slurry casting process is highly non-isothermal. The Si concentrations at the core of the α_1-Al particles in the quenched slurry samples were measured using WDS, as collated in Table IV. Taking these compositions to be a guide to the temperature of formation or homogenization in the slurry makes it possible to convert this value to a corresponding temperature using ThermoCalc™ to obtain the equilibrium temperature. The solubility limits for the four alloys are given in Table IV and in Figure 11(a). Comparison between the measured slurry temperature and the calculated temperature based on the particle core composition shows excellent agreement, suggesting that this is a reasonable approach.

Repeating this process for the core concentrations of the of the α_2-Al and α_3-Al particles also reveals a clear trend, with the α_2-Al particles forming well below the slurry forming temperature, subsequently followed by the α_3-Al particle formation. Since the size measurements of the α_2-Al and α_3-Al particles, presented in

Table IV. Measured Temperature of the Slurry and Temperature that Corresponds to the Si Concentration in the Center of Each Particle [K (°C)] Calculated Using ThermoCalc™

Alloy	T_{slurry} Measured	$C_{\text{Si}}^{\text{centre}}$ α_1-Al	T_{center}^* α_1-Al	$C_{\text{Si}}^{\text{centre}}$ α_2-Al	T_{center}^* α_2-Al	$C_{\text{Si}}^{\text{centre}}$ α_3-Al	T_{center}^* α_3-Al	$C_{\text{Si}}^{\frac{\text{dend}}{\text{root}}}$	$T_{\text{dend/root}}^*$ α_1-Al	T_{eutectic}^*
1	914 ± 1 (641 ± 1)	0.24	915 (642)	0.41	896 (623)	0.81	872 (599)	—	—	848 (575)
2	905 ± 1 (632 ± 1)	0.34	907 (634)	0.57	890 (617)	0.97	868 (595)	1.2	853 (580)	848 (575)
3	898 ± 1 (625 ± 1)	0.48	900 (627)	0.71	884 (611)	1.08	864 (591)	1.25	849 (576)	847 (574)
4	892 ± 1 (619 ± 2)	0.57	894 (621)	0.91	875 (602)	1.21	861 (588)	1.35	848 (575)	847 (574)

*Calculated using ThermoCalc™.

Table V. Nucleation Frequency n* Calculated from the Experiments and Corresponding Critical Energy for Nucleation ΔG* Calculated Using Eq. [1]

Alloy 1		Alloy 2		Alloy 3		Alloy 4	
n^*	ΔG^*	n^*	ΔG^*	n^*	ΔG^*	n^*	ΔG^*
α_2-Al	α_2-Al	α_2-Al	α_2-Al	α_2-Al	α_2-Al	α_2-Al	α_2-Al
3.4×10^{21}	$50\, k_B T_{\text{eq}}$	4.0×10^{21}	$50\, k_B T_{\text{eq}}$	4.0×10^{21}	$50\, k_B T_{\text{eq}}$	4.4×10^{21}	$50\, k_B T_{\text{eq}}$
α_3-Al	α_3-Al	α_3-Al	α_3-Al	α_3-Al	α_3-Al	α_3-Al	α_3-Al
1.7×10^{21}	$49\, k_B T_{\text{eq}}$	1.9×10^{21}	$49\, k_B T_{\text{eq}}$	1.9×10^{21}	$49\, k_B T_{\text{eq}}$	1.8×10^{21}	$49\, k_B T_{\text{eq}}$

Table II, show only small variation, this suggests two distinct and discrete events of formation. The formation of the dendritic/cellular region between the globular α_1-Al particles, Figure 5 and WDS measurements, Figure 8, is the last event before the formation of the final eutectic. This cellular growth may as such be part of the formation of the divorced eutectic microstructure.

Critical to correctly describing the formation of α_2-Al and α_3-Al particles in the rheocast samples is to explain the following three phenomena:

1. The possibility of having a discrete nucleation event despite the presence of the α_1-Al particles.
2. The lack of significant growth of the α_1-Al particles.
3. The importance of Si segregation to the liquid portion of the slurry on subsequent formation of particles.

In solidification, controlling the nucleation and approaching lower necessary undercooling in formation of primary nucleation by using different inoculant were reported.[26] The presence of particles in the melt can act as a nucleation catalysts and active nucleation sites at lower undercooling compared to homogenous nucleation. Hence, the possibility of a secondary nucleation can be analyzed using classical heterogeneous nucleation theory.[27] The nucleation frequency, n^*, for the α_2-Al and α_3-Al particles was assessed from the micrographs under the assumption of spherical and mono-sized particles, Table V. This nucleation frequency was then used to assess the critical energy for nucleation ΔG^* through

$$n^* = N_A \exp\left(-\frac{\Delta G^*}{k_B T_{\text{eq}}}\right). \qquad [1]$$

The necessary undercooling for heterogeneous nucleation is then described as[27]

$$\Delta T = \sqrt{f(\theta)\left(\frac{16\pi\sigma T_M}{3\Delta G^*}\right)\left(\frac{\sigma V_M}{\Delta H_m}\right)}, \qquad [2]$$

where T_M is the melting point; C_{eq}^L is the equilibrium concentration of Si atoms in the melt; k_B is Boltzmann's constant, 1.38×10^{-23} (m² k² K)[27]; ΔH_m is the latent heat of fusion; V_m the molar volume of the material $9,25926 \times 10^{-6}$ (m³/mol); σ is the interface energy of the interface melt/embryo 0.16 (J/m²)[28]; N_A is Avogadros number 6.022×10^{23} (1/mol); $f(\theta) = \frac{2-3\cos\theta+\cos^2\theta}{4}$ is the compensation factor for heterogeneous nucleation; and θ is the wetting angle (°).

The constants used and factors evaluated from experiments for the calculations are collated in Table V. The value for T_M is the melting temperature of the remaining melt. This choice was made as the primary α_1-Al particles do not grow during the formation of these particles and are seen as inert at this stage. The Si concentrations of the residual melt in the slurry and the associated values for T_M are collated in Table III. The nucleation temperatures for the α_2-Al and α_3-Al particles are collated in Table VI and Table VII, respectively.

The calculated undercooling based on measured Si concentration at the center of particles, Table IV, was used to fit in heterogeneous nucleation equation, Eq [2], for identifying the required contact angle for new nucleation. The wetting angles required are all low, suggesting that the effective substrates are pre-wetted. Oxide film entrainment is difficult to avoid in the RheoMetal™ process as the top surface of the melt must

Table VI. Undercooling in the Melt During Formation of α₂-Al Particles

Alloy	T_{center} [K (°C)]	Calculated Undercooling (K)	Wetting Angle Required to Achieve Undercooling, Eq. [2]
1	897 (624)	14	<22
2	891 (618)	12	<20
3	883 (610)	8	<17
4	873 (600)	3	<11

Table VII. Undercooling in the Melt During Formation of α₃-Al Particles

Alloy	T_{center} [K (°C)]	Calculated Undercooling (K)	Wetting Angle Required to Achieve Undercooling, Eq. [2]
1	872 (599)	47	<37
2	868 (595)	34	<35
3	864 (591)	28	<32
4	861 (588)	17	<25

be penetrated by the EEM. The intense shearing during stirring will deform and break up the oxide films and distribute them in the melt. Following the theory of Campbell, these oxides have one dry and one wetted surface.[29] Dihedral angles in the Al-Si system can be very low near the liquidus temperature, giving further support to the possibility of low contact angles.[30] This suggests that the formation of the α₂-Al particles is an event based on re-nucleation of the primary phase for all four alloys.

For this to be possible, the pre-existing α₁-Al particles must be regarded as inert, or only participate in the equilibration process on a significantly different time-scale than is seen in the current process. That this may be the case is supported by the apparent lack of growth of the α₁-Al particles, Table II. A slow equilibration process has also previously been reported in the literature for thixoforming of A356, giving further support to the current findings.[31] The reference for the undercooling is, as a consequence of the slow equilibration, the liquidus temperature of the remaining melt after slurry fabrication. This will decrease the apparent undercooling and as such represents a conservative measure for the characteristics of the nucleation substrate.

In die casting processes, the heat extraction rate is high and high rates of nucleation are common. Under the assumption that the primary α₁-Al particles formed in the slurry-making process and the α₂-Al particles formed through heterogeneous nucleation, an analysis of the formation of α₃-Al particles can be made. The undercooling implicitly assessed, and the required undercooling for nucleation is shown in Table VII. The observed undercooling is significantly greater than was obtained for the α₂-Al particles. The greater undercooling required suggests that the α₃-Al particles are formed on a less effective substrate, but the required contact angles are still small, and hence the nucleation substrate should also be pre-wetted. The calculated wetting angle clearly indicated the possibility of nucleation of these particles in the mold with very high cooling rate. Further investigation into this is necessary

but a possible origin may be the top surface of the melt and the surface of the EEM, leading to oxide nuclei from two different origins.

B. Formation of β(AlFeSi) and Secondary Phase

Based on the compositions of the original melt, the sequence of solidification (primary phase and eutectic reaction) was calculated using ThermoCalc™. The results are presented in Figure 12. According to the results of these calculations, needle-shaped β(AlFeSi) was the most favorable eutectic phase in all four alloys, and it forms before the eutectic Si phase. The amount of β(AlFeSi) phase is also higher than the Al-Si eutectic phase for alloys 1 to 3, in which the ratio between Fe/Si is very high. The ThermoCalc™ calculation shows good agreement with microstructural observation showing the presence of needle-shaped β(AlFeSi) with only a minute amount of Al-Si eutectic phase in alloy 1, Figure 6(a). Moreover, the temperature at which iron eutectic phase started to precipitate is close to the nucleation temperature of α₂-Al particle precipitation calculated according to the Si concentrations in the center of the α₂-Al particles, Table IV. Therefore, by decreasing temperature of the slurry to the binary eutectic temperature, β(AlFeSi) phase nucleates and in this process α₂-Al particles nucleate. The measures Si concentration and the corresponding calculated temperature in the dendrite root of disturbed α₁-Al particle in rheocast samples are close to the temperature of the ternary eutectic reaction suggesting that this morphology is formed at the very end of solidification.

C. Changes of the α₁-Al Particles During Slurry Making and Casting

1. *Homogenization the α₁-Al particles during slurry making*

During slurry making, α₁-Al particles are generated and a thermal equilibrium, the slurry temperature, is rapidly established.[21] The measurements showed that a
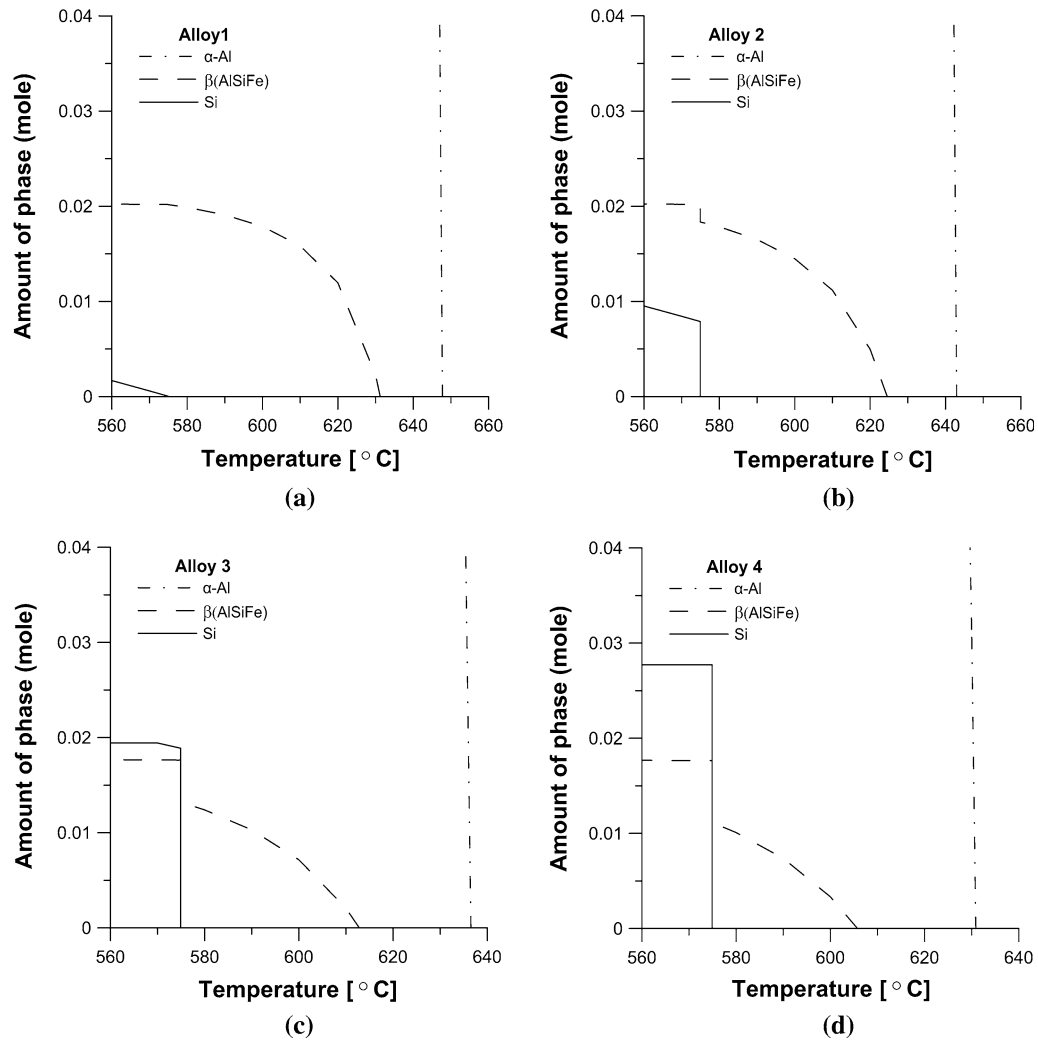
Fig. 12—Amount of secondary phases in the four alloys investigated, obtained using ThermoCalc™.

uniform distribution of Si inside the α_1-Al particles was achieved. This suggests that homogenization of the α_1-Al particles occurred during slurry making. In this context, it is important to assess if homogenization was physically possible as the RheoMetal™ is a rapid slurry-making process and hence operating far from equilibrium conditions.

A simplistic closed form solution for a spherical particle was adopted and evaluated using MATLAB™. The model consisted of a spherical particle with constant value of Si concentration at the outer boundary. The exact solution to the diffusion equation in spherical coordinates with a constant boundary composition gives the concentration in the center of the particle ($r = 0$)[32]:

$$\frac{C - C_1}{C_1 - C_0} = 1 + 2\sum_{n=1}^{\infty} (-1)^n \exp\left(\frac{-Dn^2\pi^2 t}{a^2}\right), \quad [3]$$

where C_1, C_0, and a are the initial concentration, constant concentration at the boundary of the particle, and the particle radius, respectively. The average radius for the measured particles in each alloy was

used as the input radius, a. The diffusion coefficient for Si in aluminum, D, was estimated from the following equation:

$$D_{\frac{Si}{Al}} = 2.02^{+0.97}_{-0.66}\left(\frac{(-136 \pm 3)\mathrm{kJ\,mol}^{-1}}{RT}\right)\frac{\mathrm{cm}^2}{\mathrm{s}} \quad [4]$$

in which the constants have been obtained by Fujikawa et al.[33] The measured slurry temperature was set as the input temperature, and as these constant values predict the diffusion rate at temperatures up to 893 K (620°C), by means of extrapolation the diffusion rate, $D_{Si/Al}$, for the measured temperature of slurries was calculated. The initial concentration in the α_1-Al particles, C_1, was set to the calculated solubility of Si in the aluminum phase at the liquidus temperature of each alloy, as presented in Figure 6(b). As seen in Figure 11, the solubility of Si in the aluminum phase at the liquidus temperature has been calculated as 0.16, 0.25, 0.37, and 0.47 wt pct for the alloys 1 to 4, respectively. The constant concentration at the boundary of each particle, C_0, was fixed as the solubility limit at the measured
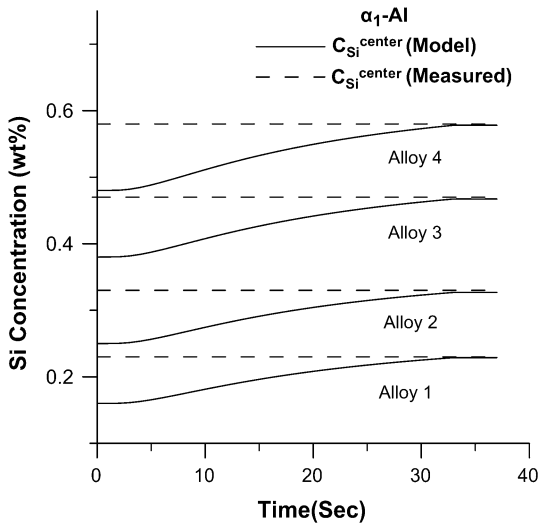
Fig. 13—Si concentration in the center of α_1-Al particle *vs* time.

slurry temperature. Using the phase diagram, the solubility of Si in the aluminum phase corresponding to the slurry temperature has been calculated to be 0.23, 0.33, 0.48, and 0.57 wt pct for alloys 1 to 4, respectively.

Figure 13 shows the evolution of the Si concentration in the center of the α_1-Al particles as a function of time. The time necessary for complete homogenization of the globular α_1-Al particles is less than 30 seconds for all alloys. The time required for the slurry making and transfer to the shot chamber for the current process set-up is in that order of magnitude. It takes about 20 seconds to make the slurry and 10 seconds for manual transfer of the melt to the shot chamber.

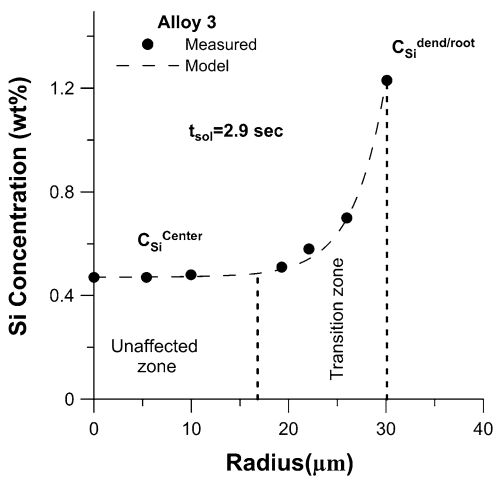### 2. Effect of cooling on solute redistribution in α_1-Al particles

The Si concentration profile in the α_1-Al particles, Figures 6(b) and 8, showed that in the as-rheocast condition, the Si concentration increased close to the particle surface. As no significant growth of α_1-Al
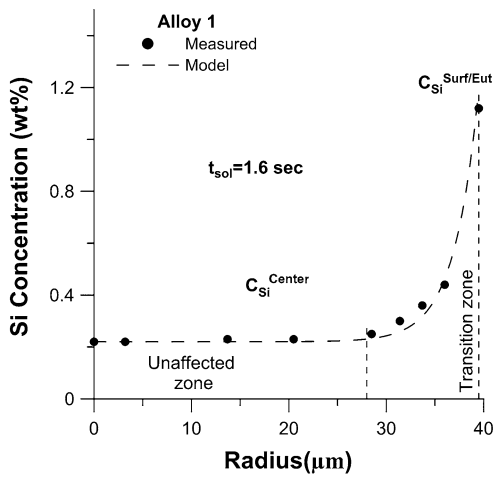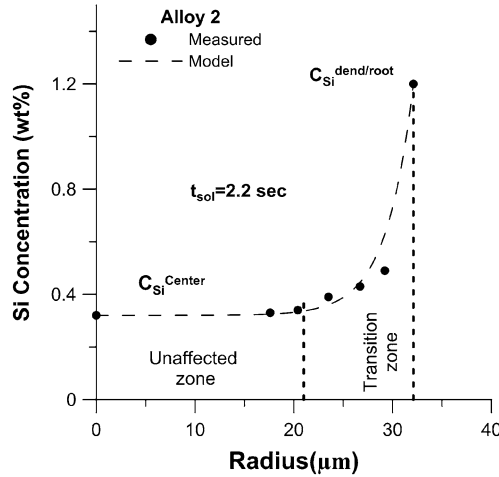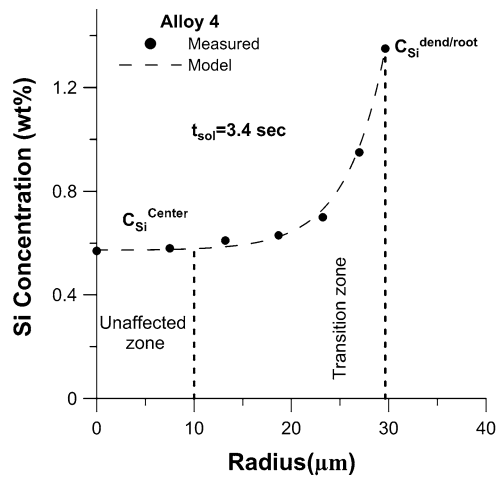

Fig. 14—The measured and calculated Si concentration profile in the transition zone in α_1-Al particle for (*a*) alloy 1 (*b*) alloy 2 (*c*) alloy 3 (*d*) alloy 4.

particles had occurred during casting of the component and solidification process, it is essential to understand if this could be the result of a back diffusion process. Based on the exact solution of the diffusion equation in spherical coordinates, the Si concentration is given by[32]

$$\frac{C - C_1}{C_1 - C_0} = 1 + \frac{2a}{\pi r} \sum_{n=1}^{\infty} \frac{(-1)^n}{n} \sin\left(\frac{n\pi r}{a}\right) \exp\left(\frac{-Dn^2\pi^2 t}{a^2}\right),$$

[5]

where r is distance from particle center. For each alloy, the measured α_1-Al particle size was used for the calculation. The initial concentration, C_1, was set as the measured Si concentration in the α_1-Al particles in the quenched slurry samples, C_{Si}^{Slurry}. The constant concentration at the particle boundary was C_0, which was set to the measured value $C_{Si}^{Surf\ Eut}$ for alloy 1 and to $C_{Si}^{dend\ root}$ for alloys 2 through 4.

The diffusivity of Si in the Al phase, $D_{Si/Al}$, was calculated using Eq. [4] for the calculated temperature corresponding to the Si concentration of the boundary at the adjacent-to-eutectic side, $C_{Si}^{Surf\ Eut}$ for alloy 1 and to the temperature corresponding to, $C_{Si}^{dend\ root}$ for alloys 2 through 4. The results are shown in Figures 14(a) through (d) for the alloys 1 to 4, respectively.

The calculated Si concentration profiles, shown as dashed lines, clearly show that the transition zone was affected by back diffusion from the higher concentration region. The time of diffusion to achieve a best fit to the measured data was 1.6, 2.2, 2.9, and 3.4 seconds for alloys 1 through 4. It can also be seen that the time of diffusion during the solidification process was not the same for the four alloys. The order of magnitude corresponds to the time for injection (1 second fill time) plus some additional time for solidification in the die cavity. An increased Si content in the transition zone of α_1-Al particles also corresponds to an increase in the amount of eutectic Al-Si phase, Figure 12, and an increase in the Si diffusivity in the aluminum phase due to increased number of vacancies.

D. Formation of the Final Invariant Eutectic

In the solidification process for the remaining melt, an invariant eutectic reaction which produces eutectic Si- and Fe-containing phases in addition to the aluminum phase will take place. The morphologies of both the β(AlFeSi) phase and the eutectic Si particles were representative for the rapid cooling conditions commonly obtained in all pressure-assisted die casting processes, Figure 5(c).[34] It should also be concluded that the deviation from spherical shape of the globular particles is a result of the increased undercooling at the end of an invariant eutectic reaction. This is supported by the fact that the concentration of Si at the root of dendritic part formed on the α_1-Al particles corresponds directly to the eutectic temperature. The α_3-Al particles are not part of the final invariant eutectic reaction as

they form well above this temperature according to Si measurement in center of these particles.

V. CONCLUSIONS

In this study, the solidification sequence in a VPDC rheocasting set-up of four Al-Si alloys from slurry fabrication and through the subsequent casting process was investigated. The microstructure of quenched samples of the slurry clearly showed that in the primary solidification stage, globular α_1-Al particles were formed during the slurry preparation process in all four alloys. The Si concentrations measured inside the α_1-Al particles show a very uniform Si distribution. The temperatures which correspond to the measured Si concentrations calculated using ThermoCalc™ were compared with the measured slurry temperatures and a good fit was found. Applying a mathematical model based on diffusion equations showed that the time to make the slurry and subsequent steps before injection into the die chamber was sufficient to homogenize Si in the α_1-Al particles. Moreover, EDS measurement on the liquid portion of the slurry indicated that the formation of these particles enriched the remaining melt, and the intensive shearing during stirring homogenized the alloying elements through this phase.

Furthermore, the microstructural evaluation based on size measurement exposed that in the microstructure of rheocast components, three types of particles α_1-Al, α_2-Al, and α_3-Al were seen. The α_1-Al particles in the range size of 60 to 75 μm formed during slurry preparation process appear to be relatively inert and do not grow or shrink during pouring into the shot sleeve and during filling and solidification process. The α_2-Al and α_3-Al particles were not observed in the quenched samples of the slurry and must therefore have formed after the slurry preparation process. Si concentrations measured in α_1-Al particles in the as-rheocast samples showed that the concentration of Si in the center of particles was similar to the concentrations measured in the α_1-Al particles in quenched slurry samples. A limited amount of back diffusion occurred in the shot chamber and in the die.

The average Si concentration in the center of α_2-Al particle showed higher values than the Si concentrations in the center of the α_1-Al particles but lower than those measured in the center of the α_3-Al particles. It was furthermore concluded that α_2-Al- and α_3-Al particles form during cooling, with the larger α_2-Al particles nucleated first at a higher temperature. Both particles formed below the temperature of the first eutectic reaction where α-Al and β(AlFeSi) precipitate as a divorced eutectic. During the final invariant reaction, the ternary eutectic consisting of α-Al, β(AlFeSi), and Si precipitated. As this reaction is an invariant reaction, undercooling can increase greatly. The observed morphological deviation of the large α_1-Al particles with a tendency to start to form dendritic or cellular features was regarded as a result of this increased undercooling.

REFERENCES

1. J.G. Kaufman and E.L. Rooy: *Aluminum Alloy Castings: Properties, Processes, and Applications*, ASM International, Material Park, 2004, pp. 7–67.
2. S. Otarawanna, C.M. Gourlay, H.I. Laukli, and A.K. Dahle: *Trans. Indian Inst. Met.*, 2009, vol. 62, pp. 499–503.
3. E.J. Vinarcik: *High Integrity Die Casting Processes*, 1st ed., Wiley, New York, 2003, pp. 13–24.
4. D.H. Kirkwood, M. Suéry, P. Kapranos, H.V. Atkinson, and K. Young: *Semi-solid Processing of Alloys*, Springer, New York, 2010, pp. 109–127.
5. M.C. Flemings, R.G. Riek, and K.P. Young: *Mater. Sci. Eng.*, 1976, vol. 25, pp. 103–17.
6. T. Li, X. Lin, and W. Huang: *Acta Mater.*, 2006, vol. 54, pp. 4815–24.
7. M. Hitchcock, Y. Wang, and Z. Fan: *Acta Mater.*, 2007, vol. 55, pp. 1589–98.
8. O. Lashkari and R. Ghomashchi: *J. Mater. Process. Technol.*, 2007, vol. 182, pp. 229–40.
9. A.K. Dahle and D.H. StJohn: *Acta Mater.*, 1999, vol. 47, pp. 31–41.
10. O. Lashkari and R. Ghomashchi: *Can. Metall. Q.*, 2014, vol. 53, pp. 47–54.
11. P. Das, S. Dutta, and S.K. Samanta: *Inst. Mech. Eng. Part B*, 2013, vol. 227, pp. 1474–83.
12. J. Wang, P. Li, G. Mi, and Y. Zhong: *J. Mater. Process. Technol.*, 2010, vol. 210, pp. 1652–59.
13. S. Nafisi and R. Ghomashchi: *JOM*, 2006, vol. 58, pp. 24–30.
14. H. Guo, X. Yang, and B. Hu: *J. Wuhan Univ. Technol. Mater. Sci. Ed.*, 2008, vol. 23, pp. 54–59.
15. S. Thanabumrungkul, S. Janudom, R. Burapa, P. Dulyapraphant, and J. Wannasin: *Trans. Nonferrous Met. Soc. China*, 2010, vol. 20, pp. s1016–s21.
16. H. Guo, X. Yang, and B. Hu: *J. Wuhan Univ. Technol. Mater. Sci. Ed.*, 2007, vol. 22, pp. 590–95.
17. J. Wannasin, R.A. Martinez, and M.C. Flemings: *Solid State Phenom.*, 2006, vols. 116–117, pp. 366–69.
18. M. Wessén and H. Cao: *A Method of and a Device for Producing a Liquid-Solid Metal Composition*, WO Patent, WO/2006/062,482.
19. M. Payandeh, A.E.W. Jarfors, and M. Wessén: *Solid State Phenom.*, 2013, vol. 192, pp. 392–97.
20. A. Jain, L. Ratke, and A. Sharma: *Trans. Indian Inst. Met.*, 2012, vol. 65, pp. 545–51.
21. O. Granath, M. Wessén, and H. Cao: *Int. J. Cast Met. Res.*, 2008, vol. 21, pp. 349–56.
22. K. Geels: *Metallographic and Materialographic Specimen Preparation, Light Microscopy, Image Analysis, and Hardness Testing*, West Conshohocken, PA, ASTM International, 2007, pp. 179–611.
23. B. Sundman, B. Jansson, and J.O. Andersson: *CALPHAD*, 1985, vol. 9, pp. 153–90.
24. J.O. Andersson, T. Helander, L. Höglund, P. Shi, and B. Sundman: *Calphad*, 2002, vol. 26, pp. 273–312.
25. H.I. Laukli, C.M. Gourlay, and A.K. Dahle: *Metall. Mater. Trans. A*, 2005, vol. 36, pp. 805–18.
26. M.P. De Cicco, L. Turng, X. Li, and J.H. Perepezko: *Metall. Mater. Trans. A*, 2011, vol. 42A, pp. 2323–30.
27. H. Fredriksson and U. Åkerlind: *Solidification and Crystallization Processing in Metals and Alloys*, Wiley, New York, 2012, pp. 179–82.
28. Z. Jian, K. Kuribayashi, and W. Jie: *Mat. Trans.*, 2002, vol. 43, pp. 721–26.
29. J. Campbell: *Complete Casting Handbook: Metal Casting Processes, Techniques and Design*, Elsevier, Oxford, 2011, pp. 19–104.
30. J.A. Bailey and J.H. Tundermann: *Trans. Metall. Soc. AIME*, 1966, vol. 236, pp. 1031–35.
31. A.E.W. Jarfors: *Int. J. Cast Met. Res.*, 2004, vol. 17, pp. 229–37.
32. J. Crank: *The Mathematics of Diffusion*, Oxford University Press, New York, 1975.
33. S. Fujikawa, K. Hirano, and Y. Fukushima: *Metall. Trans. A*, 1978, vol. 9A, pp. 1811–15.
34. S. Shin, E. Kim, G. Yeom, and J. Lee: *Mater. Sci. Eng., A*, 2012, vol. 532, pp. 151–57.